Dissecting the Balance Between Metabolic and Oncogenic Functions of Astrocyte-Elevated Gene-1/Metadherin

Yetirajam Rajesh,[1*] Saranya Chidambaranathan Reghupaty,[1*] Rachel G. Mendoza,[1] Debashri Manna,[1] Indranil Banerjee,[1] Mark A. Subler,[1] Korri Weldon,[2] Zhao Lai,[2] Shah Giashuddin,[3] Paul B. Fisher,[1,4,5] Arun J. Sanyal,[6] Rebecca K. Martin,[7] Mikhail G. Dozmorov,[8] Jolene J. Windle,[1,4] and Devanand Sarkar[1,4,5]

Obesity is an enormous global health problem, and obesity-induced nonalcoholic steatohepatitis (NASH) is contributing to a rising incidence and mortality for hepatocellular carcinoma (HCC). Increase in *de novo* lipogenesis and decrease in fatty acid β-oxidation (FAO) underlie hepatic lipid accumulation in NASH. Astrocyte-elevated gene-1/metadherin (AEG-1) overexpression contributes to both NASH and HCC. AEG-1 harbors an LXXLL motif through which it blocks activation of peroxisome proliferator activated receptor α (PPARα), a key regulator of FAO. To better understand the role of LXXLL motif in mediating AEG-1 function, using clustered regularly interspaced short palindromic repeats (CRISPR)/Cas9 technology, we generated a mouse model (AEG-1-L24K/L25H) in which the LXXLL motif in AEG-1 was mutated to LXXKH. We observed increased activation of PPARα in AEG-1-L24K/L25H livers providing partial protection from high-fat diet–induced steatosis. Interestingly, even with equal gene dosage levels, compared with AEG-1–wild-type livers, AEG-1-L24K/L25H livers exhibited increase in levels of lipogenic enzymes, mitogenic activity and inflammation, which are attributes observed when AEG-1 is overexpressed. These findings indicate that while LXXLL motif favors steatotic activity of AEG-1, it keeps in check inflammatory and oncogenic functions, thus maintaining a homeostasis in AEG-1 function. AEG-1 is being increasingly appreciated as a viable target for ameliorating NASH and NASH-HCC, and as such, in-depth understanding of the functions and molecular attributes of this molecule is essential. *Conclusion:* The present study unravels the unique role of the LXXLL motif in mediating the balance between the metabolic and oncogenic functions of AEG-1. (*Hepatology Communications* 2022;6:561-575).

Nuclear receptors mediate the action of vitamins, hormones and lipids, and function as key regulators of cell growth, differentiation, metabolism, and development.[1] These receptors are ligand-dependent transcription factors that, upon ligand-binding, recruit transcription coactivators to induce target gene transcription. The coactivators are histone acetyltransferases (HATs) that interact with the transcription factors using a specific LXXLL motif.[2] This motif is crucial for induction of nuclear receptor–mediated transcription to regulate a plethora of physiological activities. The presence of LXXLL

Abbreviations: AEG-1, astrocyte elevated gene-1; AKT, AKT serine/threonine kinase; BrdU, bromodeoxyuridine; CCND1, cyclin D1; Cpt1a, carnitine palmitoyltransferase 1a; CRISPR, clustered regularly interspaced short palindromic repeats; DNL, de novo *lipogenesis; EGF, epidermal growth factor; ERK1/2, extracellular regulated MAP kinase 1/2; FA, fatty acid; FAO, fatty acid* β*-oxidation; FASN, fatty acid synthase; FXR, farnesoid X receptor; GAPDH, glyceraldehyde 3-phosphate dehydrogenase; HCC, hepatocellular carcinoma; HFD, high-fat diet; IF, immunofluorescence; IgG, immunoglobulin G; IHC, immunohistochemistry; IL, interleukin; IP, immunoprecipitation; LPS, lipopolysaccharide; mRNA, messenger RNA; NASH, nonalcoholic steatohepatitis; NF-κB, nuclear factor kappa B; PBS, phosphate-buffered saline; PCR, polymerase chain reaction; PLIN2, perilipin-2/adipophilin; PPAR, peroxisome proliferator activated receptor; RNA-seq, RNA sequencing; RXR, retinoid X receptor; TG, triglyceride; WT, wild type.*

Received August 10, 2021; accepted October 2, 2021.

Additional Supporting Information may be found at onlinelibrary.wiley.com/doi/10.1002/hep4.1834/suppinfo.

**These authors contributed equally to this work.*

Supported by the National Cancer Institute (1R01CA230561-01A1, 1R01CA240004-01, and 1R01CA244993-01); U.S. Department of Defense (CA170048); and National Institute of Diabetes and Digestive and Kidney Diseases (1R01DK107451-01A1).

Statement of Significance: Findings identify a molecular motif that helps balance the metabolic versus oncogenic functions of AEG-1 in regulating NASH and HCC.

motif in a molecule that is not a HAT raises curiosity and prompts further analysis of its functional significance.

Astrocyte elevated gene-1 (AEG-1), also known as metadherin, is overexpressed in many common cancers, including hepatocellular carcinoma (HCC), and functions as an oncogene.[3,4] AEG-1 is a 582 a.a. protein harboring an LXXLL motif at a.a. 21-25.[5] In addition, AEG-1 has a transmembrane domain at a.a. 50-77, with which it anchors on endoplasmic reticulum (ER) membrane or cell membrane.[6,7] AEG-1 also has multiple nuclear localization signals, allowing it to translocate to the nucleus.[5,8] AEG-1 does not have any other known domains or motifs, especially any enzymatic domain. AEG-1 exerts its function by protein–protein or protein–RNA interaction. AEG-1 interacts with multiple components in the nuclear factor kappa B (NF-κB) signaling pathway, thus functioning as an essential molecule for NF-κB activation and NF-κB-induced inflammation.[9-12] ER membrane–anchored AEG-1 binds to messenger RNAs (mRNAs), especially those mRNAs that code for membrane and secreted proteins as well as ER-resident proteins, and facilitates their translation.[6,13]

Using the NH_2-terminal 1-50 a.a. peptide sequence as bait in a yeast two-hybrid assay, we previously identified that AEG-1 interacts with the nuclear receptor retinoid X receptor (RXR) using the LXXLL motif.[5] RXR heterodimerizes with one third of the 48 human nuclear receptor superfamily members, including retinoic acid receptor, thyroid hormone receptor, liver X receptor, peroxisome proliferator activated receptor (PPAR) and farnesoid X receptor (FXR), and regulates corresponding ligand-dependent gene transcription.[14] We documented that interaction of AEG-1 with RXR prevents co-activator recruitment, thereby inhibiting ligand-dependent transcription activation of RXR heterodimer partner.[5,15-17] Interestingly *in vivo*, such as in a hepatocyte-specific AEG-1 transgenic mouse (Alb/AEG-1) or a hepatocyte-specific conditional AEG-1 knockout mouse (AEG-$1^{\Delta HEP}$), this ability of AEG-1 to interfere with RXR function is specifically skewed toward PPARα, which is activated by fatty acid metabolites and functions as a master regulator of FAO.[17,18] In Alb/AEG-1 mouse,

View this article online at wileyonlinelibrary.com.
DOI 10.1002/hep4.1834

Potential conflict of interest: Dr. Sanyal consults and received grants from Conatus, Gilead, Mallinckrodt, Immuron, Boehringer Ingelheim, Novartis, Bristol-Myers Squibb, Merck, Eli Lilly, Novo Nordisk, Fractyl, Siemens, Madrigal, Inventiva, and Covance. He consults and owns stock in Genfit. He consults for Intercept, Pfizer, Salix, Galectin, Hemoshear, Terns, Albireo, Sanofi, Janssen, Takeda, Northsea, AMRA, Perspectum, Poxel, 89 Bio, AstraZeneca, NGM, Amgen, Regeneron, Genentech, Roche, Prosciento, Histoindex, Path AI, and Biocellvia. He received grants from Echosens-Sandhill, Owl, and Second Genome. He owns stock in Exhalenz, Sanyal Bio, Durect, Indalo, Tiziana, and Rivus. He received royalties from Elsevier and UptoDate.

ARTICLE INFORMATION:

From the [1]Department of Human and Molecular Genetics, Virginia Commonwealth University, Richmond, VA, USA; [2]Greehey Children's Cancer Research Institute, University of Texas Health Science Center San Antonio, San Antonio, TX, USA; [3]Department of Pathology and Laboratory Medicine, New York Presbyterian Health System at Weill Cornell Medical College, New York, NY, USA; [4]Massey Cancer Center, Virginia Commonwealth University, Richmond, VA, USA; [5]VCU Institute of Molecular Medicine, Virginia Commonwealth University, Richmond, VA, USA; [6]Department of Internal Medicine, Virginia Commonwealth University, Richmond, VA, USA; [7]Department of Microbiology and Immunology, Virginia Commonwealth University, Richmond, VA, USA; [8]Department of Biostatistics, Virginia Commonwealth University, Richmond, VA, USA.

ADDRESS CORRESPONDENCE AND REPRINT REQUESTS TO:

Devanand Sarkar, M.B.B.S., Ph.D
Department of Human and Molecular Genetics
Virginia Commonwealth University
1220 East Broad Street
PO Box 980035
Richmond, VA 23298, USA
E-mail: devanand.sarkar@vcuhealth.org
Tel.: +1-804-827-2339

PPARα activation and FAO are inhibited, resulting in spontaneous nonalcoholic steatohepatitis (NASH), which is reversed in AEG-$1^{\Delta HEP}$ mouse, thereby providing protection from high-fat diet (HFD)–induced NASH.[17]

To obtain better insights into the mechanism by which the LXXLL motif regulates AEG-1 function, using the CRISPR/Cas9 technique,[19] we generated a mouse model (AEG-1-L24K/L25H) in which the LXXLL motif in AEG-1 was mutated to LXXKH. This mutant mouse facilitates analysis of the balance between metabolic and oncogenic functions of AEG-1 and unravels aspects of regulation of AEG-1 function contributing to NASH and HCC.

Materials and Methods

CONSTRUCTION OF AEG-1-L24K/L25H MICE

AEG-1-L24K/L25H mice were created in C57BL/6/J background using CRISPR/Cas9 technology,[19] and the targeting strategy is shown in Fig. 1A,B. AEG-1-L24K/L25H heterozygote x heterozygote mating was performed to generate AEG-1–wild-type (WT) and AEG-1-L24K/L25H littermates. Mice were genotyped using an allele-specific polymerase chain reaction (PCR) strategy (Fig. 1C). This strategy involved two separate PCR reactions using a common forward primer paired with either an L24K/L25H-specific reverse primer or a WT-specific reverse primer, yielding a 403-bp product size in either case. An internal control primer pair (LIN52), generating a 703-bp product, was included in all reactions. The sequences of the primers are AEG-1-WT forward: 5′-ATTGTTCCGCCGGGGGAGGAC-3′; AEG-1-WT reverse: 5′-AAACCTAGGCCGACC GAGAGCAA-3′; AEG-1-L24K/L25H reverse: 5′-AAACCTAGGCCGAC**G**GA**AT**GC**TT**-3′; LIN52 forward: 5′-TTGAGACCTGACTTTCTT AAACAC-3′; and LIN52 reverse: 5′-TTCCTGTG TGATATACATGCAGAC-3′. The mutated bases are shown in bold.

Mice were fed regular chow. For HFD experiments, 8-week old mice were fed a high-fat and cholesterol-containing diet (TD.88137; Harlan Laboratories, Indianapolis, IN) for 20 weeks. This diet contains 0.2% total cholesterol and 21% total fat by weight, which provides 42% kcal (4.5 kcal/g). All animal studies were approved by the Institutional Animal Care and Use Committee at Virginia Commonwealth University.

ISOLATION AND CULTURE OF PRIMARY HEPATOCYTES

Primary mouse hepatocytes were isolated and cultured as previously described.[20] The hepatocytes were used immediately after isolation in-house and were mycoplasma-free as detected by Mycoplasma Detection Kit (Thermo Fisher Scientific, Waltham, MA). Hepatocytes were treated with a PPARα-agonist CP775146 (2.5 μM) for 24 hours, with lipopolysaccharide (LPS, 100 ng/mL) for 24 hours, and with epidermal growth factor (epidermal growth factor [EGF], 50 ng/mL) for 15 minutes.

CELL VIABILITY, BROMODEOXYURIDINE INCORPORATION, SENESCENCE-ASSOCIATED β-GALACTOSIDASE, AND LUCIFERASE REPORTER ASSAYS

Hepatocytes (1×10^3) were plated in each well of a 96 well plate for measuring viability by a standard 3-(4,5-dimethylthiazol-2-yl)-2,5-diphenyltetrazolium bromide assay.[21] Bromodeoxyuridine (BrdU) incorporation was measured using BrdU Cell Proliferation Assay Kit (#6813; Cell Signaling Technology, Danvers, MA) according to the manufacturer's protocol. Hepatocytes were cultured for 7 days, and senescence-associated β-galactosidase activity was measured as described.[21] NF-κB luciferase reporter assay was performed as described.[12]

RNA IMMUNOPRECIPITATION, TOTAL RNA EXTRACTION, COMPLEMENTARY DNA PREPARATION, AND REAL TIME PCR

RNA immunoprecipitation using lysates from AEG-1-WT and AEG-1-L24K/L25H livers and control immunoglobulin G (IgG) and anti-AEG-1 antibody (rabbit polyclonal; in-house) was performed using

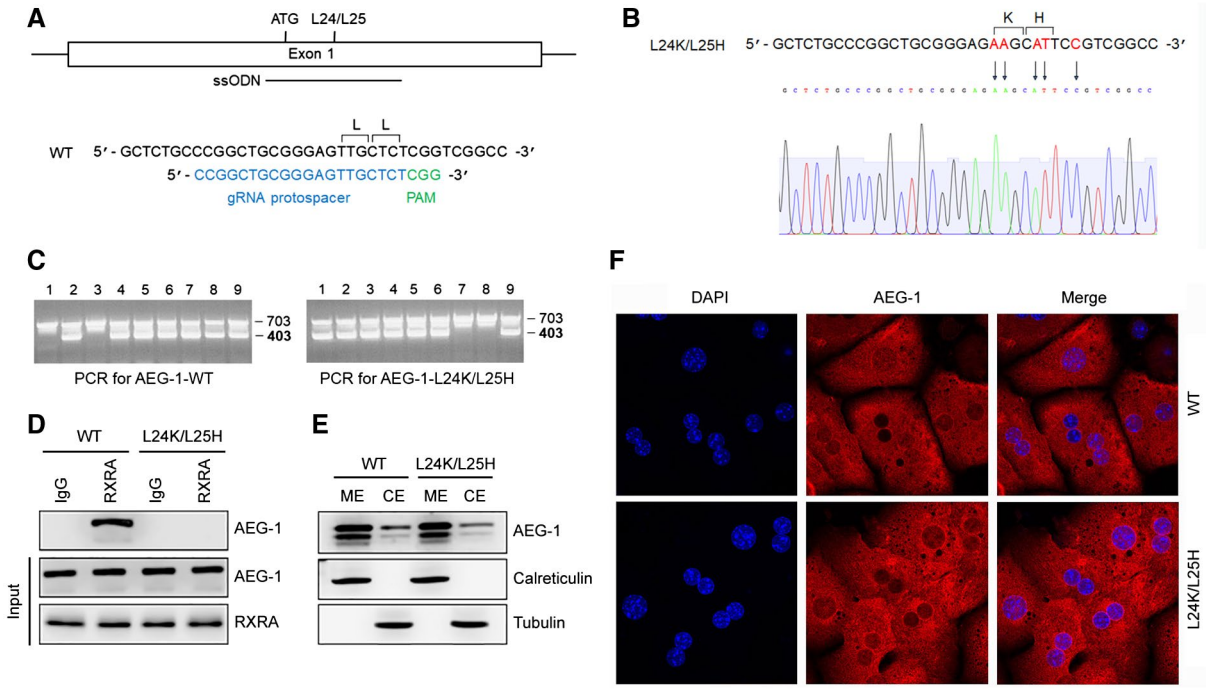

FIG. 1. Generation of AEG-1-L24K/L25H mouse. (A) Top: Diagram of AEG-1 exon 1, indicating the location of the ATG start codon, amino acids L24 and L25, and the location of the 200-nt antisense ssODN repair template used for targeting. Bottom: Sequence of the WT AEG-1 allele; sequence of the gRNA protospacer (blue) and the PAM (green). (B) Top: Sequence of the L24K/L25H allele with the nucleotide changes introduced to create the amino acid substitutions and destroy the PAM sequence shown in red. Bottom: Partial sequencing chromatograph from a homozygous AEG-1-L24K/L25H mouse corresponding to the same region shown in top panel. Arrows indicate the location of the nucleotide substitutions. (C) Genotyping of AEG-1-L24K/L25H mice. Nine pups generated from an AEG-1-L24K/L25H heterozygote x heterozygote mating were genotyped using an allele-specific PCR strategy. This strategy involved two separate PCR reactions using a common forward primer paired with either a WT-specific reverse primer or an L24K/L25H-specific reverse primer, yielding a 403-bp product size, in either case. An internal control primer pair (LIN52), generating a 703-bp product, was included in all reactions. Mice 1 and 3 from this litter are homozygous L24K/L25H, mice 2, 4-6, and 9 are heterozygotes, and mice 7 and 8 are WT. The PCR product from mouse 3 was sequenced to generate the chromatograph shown in (B). (D) AEG-1-WT and AEG-1-L24K/L25H liver extracts (1 mg each) were subjected to immunoprecipitation using anti-RXRA antibody, and western blot was performed using anti-AEG-1 antibody. Five percent input was used for western blot for AEG-1 and RXRA. (E) Western blot for the indicated proteins in membrane (ME) and cytosolic (CE) fractions extracted from AEG-1-WT and AEG-1-L24K/L25H livers. (F) IF analysis of AEG-1 expression in AEG-1-WT and AEG-1-L24K/L25H primary hepatocytes. The image was analyzed by a confocal laser scanning microscope. Magnification, ×630.

Magna RIP RNA Binding Protein Immunoprecipitation kit (Millipore, Burlington, MA) according to the manufacturer's protocol, and RNA was extracted from the immunoprecipitates using the QIAGEN miRNAeasy Mini Kit (QIAGEN, Valencia, CA). Total RNA from livers and hepatocytes was extracted using the same kit. Complementary DNA preparation was done using ABI cDNA synthesis kit (Applied Biosystems, Foster City, CA). Quantitative real-time PCR was performed using an ABI ViiA7 fast real-time PCR system and Taqman gene-expression assays according to the manufacturer's protocol (Applied Biosystems).

RNA SEQUENCING

Total RNA, extracted using the Qiagen miRNAeasy mini kit from hepatocytes, was used for RNA sequencing (RNA-seq). The RNA-seq library was prepared using an Illumina TruSeq RNA sample preparation kit and subjected to two rounds of sequencing on the Illumina HiSeq3000 platform (San Diego, CA). The RNA-seq libraries were pooled together to aim about 25-40 million reads passed the filter per sample. All sequencing reads were quality controlled using FastQC v0.11.2. Illumina adapters

were trimmed using Cutadapt v1.9.dev2, and replicates were merged and aligned with their reference genome (UCSC mouse genome build mm10) using subread-align v1.4.6-p4. The BAM files from alignment were processed using featureCounts v1.4.6-p4 to obtain the counts per gene in all samples. The Mus_musculus.GRCm38.83.gtf gene definition file was used. The differential expression analysis was performed using edgeR v3.18.1. Genes having counts per million less than two in all samples were excluded. Differentially expressed genes were defined using $P < 0.01$ and false discovery rate (FDR)–corrected $P < 0.1$ cutoffs. All bioinformatics analyses were conducted in the R/Bioconductor computing environment v3.4.0. The GEO Series accession number of this data set is GSE156849.

IMMUNOPRECIPITATION AND WESTERN BLOT ANALYSIS

Cell lysates and tissue extracts were prepared and western blotting was performed as described.[12] Membrane and cytosolic fractions were prepared from liver tissues using a kit from MyBioSource (San Diego, CA) according to the manufacturer's instructions. Immunoprecipitation was performed using liver extracts and anti-RXRA antibody (rabbit polyclonal; 1:100) or anti-AEG-1 antibody (chicken polyclonal: 1:500). The primary antibodies used were anti-AEG-1 (chicken; in-house; 1:5,000), anti-p-ERK (rabbit; Cell Signaling #4377S; 1:1,000), anti-ERK (rabbit; Cell Signaling #4695S; 1:1,000), anti-p–AKT serine/threonine kinase (AKT; rabbit; Cell Signaling #XP4060S; 1:1,000), anti-AKT (rabbit; Cell Signaling #9272S; 1:1,000), anti–acetyl co-A carboxylase alpha (ACACA; rabbit; Cell Signaling #3676S; 1:1,000), anti–fatty acid synthase (FASN; rabbit; Cell Signaling #3180S; 1:1,000), anti–stearoyl–coenzyme A desaturase 1 (SCD1; rabbit; Cell Signaling #2794S; 1:1,000), anti–stearoyl–coenzyme A desaturase 2 (SCD2; mouse; Santa Cruz #518034; 1:1,000), anti–3-hydroxy-3-methylglutaryl-CoA reductase (HMGCR; rabbit; Santa Cruz #33827; 1:1,000), anti–3-hydroxy-3-methylglutaryl-CoA synthase 1 (HMGCS1; rabbit; Bethyl Laboratories #A304-590A; 1:2,000), anti–sterol regulatory element binding protein 1 (SREBP1; rabbit; Santa Cruz #365513; 1:1,000), anti–sterol regulatory element binding protein 2 (SREBP2; mouse; Santa Cruz #271615; 1:1,000), anti-cyclin D1 (CCND1; rabbit; Cell Signaling #2978S; 1:1,000), anti-cyclin E (mouse; Oncogene Research Products #Ab-1 CC05; 1:1,000), anti-RXRA (rabbit; Santa Cruz #553; 1:1,000), anti-p65 (rabbit; Cell Signaling #3034; 1:1,000), and anti–glyceraldehyde 3-phosphate dehydrogenase (GAPDH) (mouse; Santa Cruz #166545; 1:1,000). Densitometric analysis was performed using ImageJ software (National Institutes of Health).

IMMUNOHISTOCHEMISTRY AND IMMUNOFLUORESCENCE ASSAYS

Immunohistochemistry (IHC) was performed on formalin-fixed paraffin-embedded sections as described,[12] using anti–perilipin-2/adipophilin (PLIN2; rabbit; Novus Biologicals #NB110-40877; 1:200); F4/80 antibody (rat; Bio-Rad #MCA497R; 1:100), and anti-neutrophil antibody (rat; Abcam #ab2557; 1:200). Hepatocytes were cultured in collagen-1-coated four-chamber slides, and immunofluorescence (IF) was performed using anti-AEG-1 antibody (chicken; in-house; 1:400) as described.[22] For IHC, images were analyzed using an Olympus microscope. For IF, images were analyzed using a Zeiss confocal laser scanning microscope.

IMMUNE CELL ANALYSIS BY FLOW CYTOMETRY

Livers were perfused with phosphate-buffered saline (PBS) and harvested. The gallbladder was removed, and the liver tissue was finely minced and immersed in digestion buffer (Collagenase D; Roche and DNase I; Sigma, St. Louis, MO) for 40 minutes at 37°C. After digestion, livers were filtered, washed, and subjected to a slow (30*g* for 5 minutes) spin to settle debris and dead cells. The liquid component was transferred to a new tube and subjected to a normal spin (350*g* for 5 minutes). Pelleted cells were then washed in PBS and stained for flow cytometry. Live/dead exclusion stain was performed per manufacturer's directions (Zombie NIR; BioLegend, San Diego, CA). Cells were washed, and Fc receptors were blocked (2.4G2; in-house) and stained in Brilliant Violet Stain Buffer (BD Biosciences, Franklin Lakes, NJ) for 30 minutes on ice in the dark. The stains used were BUV395 conjugated anti-mouse CD11b, BUV661 conjugated anti-mouse

CD8, BV421 conjugated anti-mouse CD4, BV510 conjugated anti-mouse F4/80, BV605 conjugated anti-mouse CD11c, BV650 conjugated anti-mouse CD19, BV711 conjugated anti-mouse CD44, fluorescein isothiocyanate conjugated anti-mouse Ly6G, PE/Cy7 conjugated anti-mouse CD62L, Alexa Fluor 700 conjugated anti-mouse TCRbeta, and PE Dazzle 594 conjugated anti-mouse CD45 (all from BioLegend or BD Biosciences). Cells were washed, fixed with Fixation Buffer (BioLegend) for 15 minutes at room temperature, washed again, and resuspended in PBS for analysis. All acquisitions were performed on the Cytek Aurora 5 laser instrument (Cytek, Fremont, CA) in the Massey Cancer Center Flow Cytometry Shared Resource at Virginia Commonwealth University, and data were analyzed in FlowJo v.10.8.0 (BD Biosciences).

MEASUREMENT OF HEPATIC TRIGLYCERIDES AND CHOLESTEROL

Hepatic lipids were extracted using the Folch extraction method, and triglycerides (TGs) and cholesterol were measured using the chemical method by the University of Cincinnati Mouse Metabolic Phenotyping Center.

STATISTICAL ANALYSIS

Data are represented as the mean ± SEM and analyzed for statistical significance using one-way analysis of variance followed by Newman-Keuls test as a *post hoc* test. A P value of < 0.05 was considered as significant.

Results

To better understand the role of LXXLL motif in mediating AEG-1 function, we generated a mutant knock-in mouse in C56BL/6/J background in which LXXLL motif of AEG-1 was mutated to LXXKH (AEG-1-L24K/L25H) using CRISPR/Cas9 technology. The targeting strategy to generate the mouse is shown in Fig. 1A,B. AEG-1-L24K/L25H heterozygote x heterozygote breeding allowed us to obtain homozygote AEG-1-WT and AEG-1-L24K/L25H littermates, which were used in all subsequent experiments (Fig. 1C). Immunoprecipitation (IP) assay using anti-RXRA antibody showed loss of interaction in AEG-1-L24K/L25H compared with AEG-1-WT (Fig. 1D). Western blot documented that both AEG-1-WT and AEG-1-L24K/L25H proteins are predominantly localized in calreticulin-positive membrane fraction, indicating their localization in the ER (Fig. 1E). IF studies in primary hepatocytes confirmed that the localization of AEG-1-L24K/L25H protein was similar to AEG-1-WT protein (Fig. 1F).

We treated AEG-1-WT and AEG-1-L24K/L25H hepatocytes with a PPARα-agonist CP775146 (2.5 μM) and analyzed global gene-expression changes in naïve and CP775146-treated hepatocytes by RNA-seq. Using a very stringent FDR of < 0.0001 and P value of < E-5, 1,440 genes showed up-regulation and 1,355 genes showed down-regulation in naïve AEG-1-L24K/L25H hepatocytes compared with AEG-1-WT. Comparison of differentially modulated Kyoto Encyclopedia of Genes and Genomes pathways between naïve AEG-1-WT and AEG-1-L24K/L25H hepatocytes identified several metabolic pathways with high significance (Fig. 2A). Most importantly, PPAR signaling pathway and fatty acid (FA) degradation were identified to be differentially modulated. We focused on PPARα target genes with special emphasis on those genes that regulate FAO. Indeed, both basal and CP775146-induced expression of PPARα target genes were significantly higher in AEG-1-L24K/L25H hepatocytes compared with WT (Fig. 2B). Carnitine palmitoyltransferase 1a (Cpt1a) is a transporter allowing transport of FAs to mitochondria for β-oxidation, and therefore serves as the rate-limiting molecule in this process. We validated changes in Cpt1a and acyl-coA oxidase 1 (Acox1, regulating peroxisomal FAO) level by Taqman quantitative real-time PCR, showing significantly higher basal and CP775146-induced expression in AEG-1-L24K/L25H hepatocytes compared with AEG-1-WT (Fig. 2C).

The gene-expression data from the naïve AEG-1-WT and AEG-1-L24K/L25H hepatocytes were further analyzed by Ingenuity Pathway Analysis to identify the upstream regulators, the activation or inhibition of which might lead to alterations in downstream genes. An activation z-score >2 indicates activation, and a score of <–2 indicates inhibition. A P-value cutoff of E-10 was used for stringent analysis. These upstream regulators that are activated or

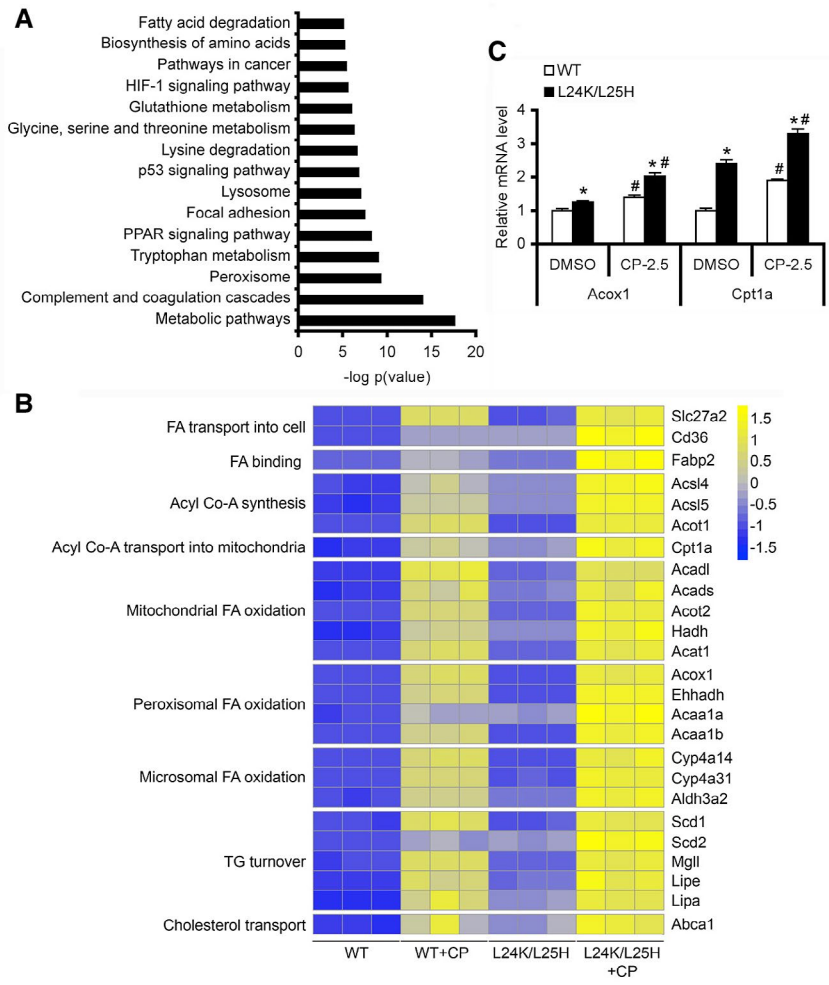

FIG. 2. PPARα is activated in AEG-1-L24K/L25H hepatocytes. (A) Kyoto Encyclopedia of Genes and Genomes pathways activated in naïve AEG-1-L24K/L25H primary hepatocytes were deduced using differentially expressed genes identified by RNA-seq. (B) Heatmap of PPARα-target genes in naïve and CP775146-treated AEG-1-WT and AEG-1-L24K/L25H hepatocytes. (C) Expression analysis by quantitative real-time PCR of Cpt1a and Acox1 mRNAs in DMSO-treated and CP775146-treated AEG-1-WT and AEG-1-L24K/L25H hepatocytes. Normalized by GAPDH. Expression level in DMSO-treated AEG-1-WT was considered as 1 for each gene. Data represent mean ± SEM of at least triplicate experiments. $^{*}P < 0.05$ versus corresponding AEG-1-WT; $^{\#}P < 0.05$ versus corresponding DMSO-treated AEG-1-WT or CP775146-treated AEG-1-WT. Abbreviations: Abca1, ATP binding cassette subfamily A member 1; Acaa1a, acetyl-CoA acyltransferase 1A; Acaa1b, acetyl-CoA acyltransferase 1B; Acadl, Acyl-CoA dehydrogenase, long chain; Acads, Acyl-CoA dehydrogenase, short chain; Acat1, Acetyl-CoA acetyltransferase 1; Acot1, Acyl-CoA thioesterase 1; Acot2, Acyl-CoA thioesterase 2; Acox1, Acyl-CoA oxidase 1; Acsl4, Acyl-CoA synthetase long chain family member 4; Acsl5, Acyl-CoA synthetase long chain family member 5; Aldh3a2, Aldehyde dehydrogenase 3 family member A2; Cd36, Cd36 molecule; Cpt1a, Carnitine palmitoyltransferase 1a; Cyp4a14, Cytochrome P450, family 4, subfamily a, polypeptide 14; Cyp4a31, Cytochrome P450, family 4, subfamily a, polypeptide 31; Ehhadh, Enoyl-CoA hydratase and 3-hydroxyacyl CoA dehydrogenase; Fabp2, Fatty acid binding protein 2; Hadh, Hydroxyacyl-CoA dehydrogenase; Lipa, Lipase A, lysosomal acid type; Lipe, Lipase E, hormone sensitive type; Mgll, Monoglyceride lipase; Scd1, Stearoyl-Coenzyme A desaturase 1; Scd2, Stearoyl-Coenzyme A desaturase 2; Slc27a2, Solute carrier family 27, member a2.

inhibited in the AEG-1-L24K/L25H group could be clustered into three broad functional categories (Table 1): (1) Activation of nuclear receptors: PPARα as well as its agonists (pirinixic acid, fenofibrate, benzafibrate) and cholic acid, which is an activator of FXR; (2) promotion of tumorigenesis: mitogenic signaling that includes ERBB2 (erb-b2 receptor tyrosine kinase 2)/EGFR (epidermal growth factor receptor) and downstream molecules such as RABL6 (RAB, member RAS oncogene family like 6), RAF1 (Raf-1

TABLE 1. UPSTREAM REGULATORS OF DIFFERENTIALLY EXPRESSED GENES IN AEG-1-L24K/L25H HEPATOCYTES

Upstream Regulator	z-Score	*P* Value	Mechanism	Consequence
PPARA	3.106	1.56E-52	Activation of PPARα	Increased FAO
Pirinixic acid (PPARα agonist)	3.343	4.51E-49		
Benzafibrate (PPARα agonist)	2.35	3.09E-13		
Fenofibrate (PPARα agonist)	2.343	1.31E-17		
Cholic acid	2.854	3.35E-11	Activation of FXR	Bile acid signaling
ERBB2	3.985	5.94E-43	Increased mitogenic signaling	Promotion of tumorigenesis
RAF1	3.653	1.57E-14		
EGFR	2.371	4.25E-14		
ERK1/2	2.113	2.46E-12		
MAP2K1	2.548	4.06E-10		
RABL6	4.229	6.68E-18		
PD98059 (MEK/ERK inhibitor)	–2.593	3.56E-22		
LY294002 (PI3K/Akt inhibitor)	–2.91	2.92E-15		
Let-7 (miRNA targeting RAS)	–4.345	1.3E-13		
Genistein (EGFR inhibitor)	–2.717	1.54E-13		
HGF	4.681	2.18E-32	Increased mitogenic signaling, EMT	
VEGF	4.519	2.22E-27	Increased angiogenesis	
EGLN	3.679	6.95E-19		
CCND1	3.035	9.86E-24	Cell cycle progression	
E2F1	2.575	2.94E-13		
FOXM1	2.099	1.44E-11		
CDKN1A	–2.449	9.58E-19		
CDKN2A	–2.448	1.74E-11		
SMARCB1	–3.161	2.17E-27	Tumor formation by a variety of mechanisms	
Methapyrilene	3.363	4.63E-20		
TBX2	5.088	8.11E-16		
MITF	2.1	1.74E-14		
miR-124-3p	–3.491	2.35E-15		
F2 (thrombin)	3.63	1.63E-13	Increased coagulation, invasion, and metastasis	
F2R (thrombin receptor)	2.718	2.14E-11		
NFE2L2	2.163	3.94E-21	Protection from oxidative stress	
LPS	3.516	2.53E-38	NF-κB activation	Increased inflammation
NFkB (complex)	2.152	2.22E-12		
RELA	2.133	9.61E-10		
IFNG	2.828	5.95E-24	Macrophage activation	
CSF2	4.034	4.03E-18		
Dexamethasone	–2.985	8.76E-49	Activation of glucocorticoid receptor	
Triamcinolone acetonide	–3.044	1.42E-10		
Valproic acid	–2.289	1.42E-15	Increased histone acetylation	Epigenetic gene regulation
KDM5B	–3.954	8.93E-12	Increased lysine methylation	

Abbreviations: CDKN1A/2A, cyclin dependent kinase inhibitor 1A/2A; CSF2, colony stimulating factor 2; E2F1, E2F transcription factor 1; EGFR, epidermal growth factor receptor; EGLN, Egl-9 family hypoxia inducible factor; EMT, epithelial-to-mesenchymal transition; ERBB2, erb-b2 receptor tyrosine kinase 2; FOXM1, forkhead box M1; HGF, hepatocyte growth factor; IFNG, interferon gamma; MAP2K1, mitogen-activated protein kinase 1; MITF, melanocyte inducing transcription factor; miRNA, microRNA; NFE2L2, nuclear factor, erythroid 2 like 2; PI3K, phosphotidylinositol 3-kinase ; RABL6, RAB, member RAS oncogene family like 6; RAF1, Raf-1 proto-oncogene, serine/threonine kinase; RELA, reticuloendotheliosis viral oncogene homolog A, NF-κB subunit; TBX2, T-box transcription factor 2; and VEGF, vascular endothelial growth factor.

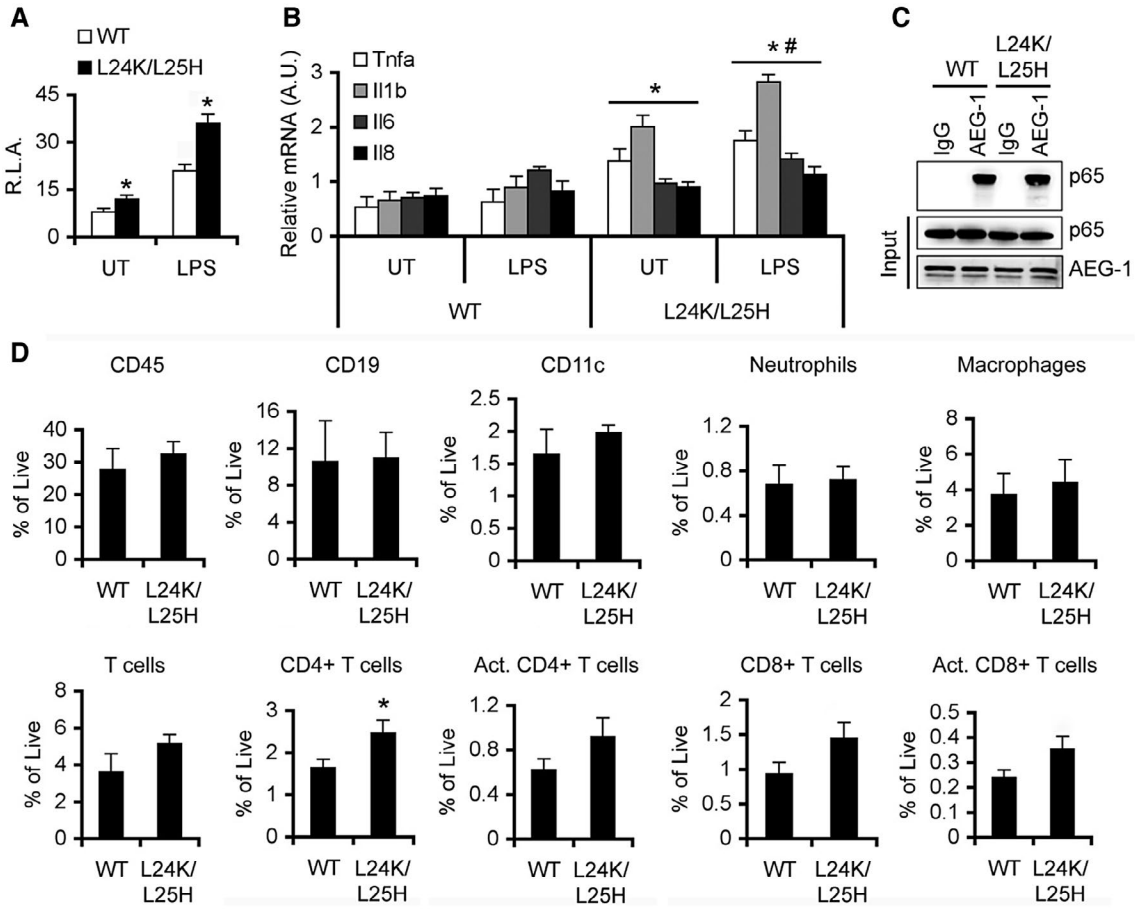

FIG. 3. AEG-1-L24K/L25H induces inflammation. (A) NF-κB luciferase reporter activity was measured in AEG-1-WT and AEG-1-L24K/L25H primary hepatocytes treated or not with LPS (100 ng/mL) for 24 hours. Firefly luciferase activity was normalized by Renilla luciferase activity. The activity of empty pGL3-basic vector was considered as 1. Data represent mean ± SEM of three independent experiments. **P* < 0.05 versus corresponding AEG-1-WT. (B) AEG-1-WT and AEG-1-L24K/L25H primary hepatocytes were treated with LPS (100 ng/mL) for 24 hours, and the expression of the indicated genes was analyzed by Taqman quantitative real-time PCR. Normalized by GAPDH. Data represent mean ± SEM of at least triplicate experiments. **P* < 0.05 versus untreated (UT) AEG-1-WT; #*P* < 0.05 versus LPS-treated AEG-1-WT. (C) AEG-1-WT and AEG-1-L24K/L25H liver extracts (1 mg each) were subjected to IP using anti-AEG-1 antibody, and western blot was performed using anti-p65 antibody. Five percent input was used for western blot for p65 and AEG-1. (D) Analysis of immune cells in naïve livers of AEG-1-WT (n = 3) and AEG-1-L24K/L25H (n = 4) littermates by flow cytometry. Data represent mean ± SEM. **P* < 0.05. Abbreviation: R.L.A., relative luciferase activity.

proto-oncogene, serine/threonine kinase), MAP2K1 (mitogen-activated protein kinase 1), and ERK1/2 (extracellular regulated MAP kinase 1/2), and inhibition of microRNA let-7, which targets Ras, inhibition of ERK1/2 inhibitor PD98059, and inhibition of phosphotidylinositol 3-kinase (PI3K)/AKT inhibitor LY294002; cell cycle acceleration that includes CCND1, E2F1 (E2F transcription factor 1), FOXM1 (forkhead box M1), and inhibition of CDKN1A (cyclin dependent kinase inhibitor 1A; p21) and CDKN2A (cyclin dependent kinase inhibitor 2A; p16); invasion and metastasis that include HGF (hepatocyte growth factor), coagulation factors such as thrombin and its receptor (F2 and F2R), and inhibition of SPARC (secreted protein acidic and cysteine rich); angiogenesis that includes VEGF (vascular endothelial growth factor), NFE2L2 (nuclear factor, erythroid 2 like 2), and EGLN (Egl-9 family hypoxia inducible factor); and general tumorigenic factors such as TBX2 (T-box transcription factor 2) and MITF (melanocyte inducing transcription factor); and (3) increased inflammation: activation of NF-κB that includes LPS, NF-kB

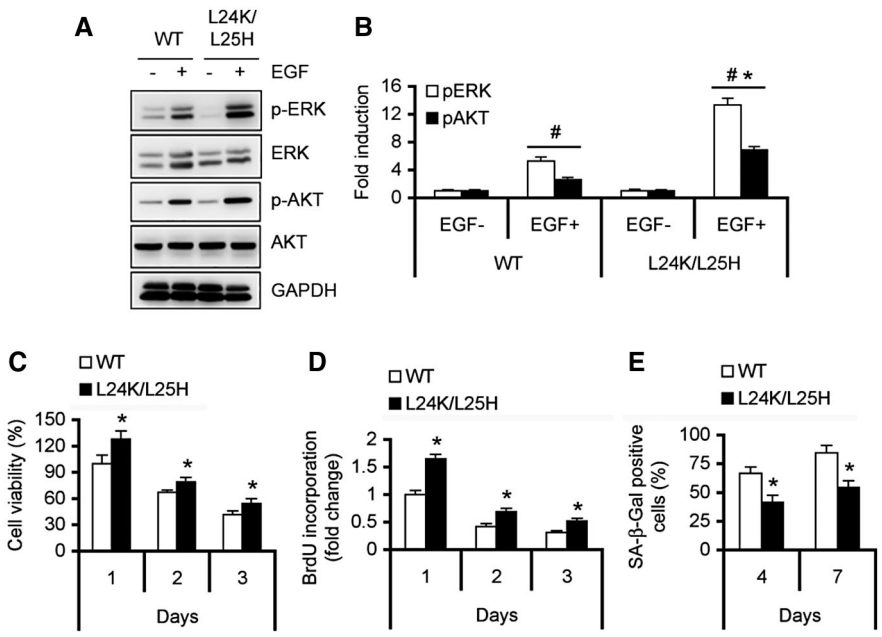

FIG. 4. Mitogenic pathways are activated in AEG-1-L24K/L25H hepatocytes. (A) AEG-1-WT and AEG-1-L24K/L25H primary hepatocytes were treated with EGF (50 ng/mL) for 15 minutes, and the expression of the indicated proteins was analyzed by western blot. A representative image is shown. GAPDH was used as loading control. (B) Graphical representation of densitometric analysis of western blot shown in (A). Data represent mean ± SEM of at least triplicate independent experiments performed with hepatocytes isolated from littermates. $^{\#}P < 0.01$ versus corresponding EGF-; $^{*}P < 0.01$ versus WT-EGF+. (F-H) Cell viability by 3-(4,5-dimethylthiazol-2-yl)-2,5-diphenyltetrazolium bromide assay (C), BrdU incorporation (D), and senescence-associated β-galactosidase–positive cells (E) were determined in AEG-1-L24K/L25H and AEG-1-WT primary hepatocytes at the indicated time points. Data represent mean ± SEM of at least triplicate independent experiments performed with hepatocytes isolated from littermates. $^{*}P < 0.05$ versus AEG-1-WT. Abbreviation: SA-β-Gal, senescence-associated β-galactosidase.

(complex), and RelA (reticuloendotheliosis viral oncogene homolog A, NF-κB subunit) and inhibition of dexamethasone and triamcinalone; activation of macrophages such as CSF2 (colony stimulating factor 2) and IFNG (interferon gamma).

To confirm the observations from RNA-seq analysis, NF-κB luciferase reporter activity in primary hepatocytes isolated from AEG-1-WT and AEG-1-L24K/L25H mice was measured. Both basal and LPS-induced NF-κB activity was significantly higher in AEG-1-L24K/L25H hepatocytes compared with AEG-1-WT hepatocytes (Fig. 3A). Primary hepatocytes were treated with LPS, and the expression of inflammatory cytokines, tumor necrosis factor α, interleukin (IL)-1β, IL-6, and IL-8 were measured by quantitative real-time PCR. Both basal and LPS-induced levels of these cytokines were significantly higher in AEG-1-L24K/L25H hepatocytes versus AEG-1-WT, establishing their pro-inflammatory phenotype (Fig. 3B). In IP assay with equal amount of AEG-1 and p65 NF-κB in the input, compared with AEG-1-WT, AEG-1-L24K/L25H showed increased binding to p65 NF-κB (1.5 fold) (Fig. 3C). We analyzed the inflammatory cell population in naïve livers from AEG-1-WT and AEG-1-L24K/L25H littermates by flow cytometry analysis. There was a statistically significant increase in CD4+ T cells in AEG-1-L24K/L25H livers compared with AEG-1-WT (Fig. 3D). In addition, there was an increasing trend, although not statistically significant, for CD11c+ dendritic cells, CD11b+ macrophages, and activated CD4+, CD8+, and activated CD8+ T cells, in AEG-1-L24K/L25H livers versus AEG-1-WT (Fig. 3D). Collectively, these findings demonstrate that AEG-1-L24K/L25H creates an inflammatory milieu in the liver.

To check mitogenic ability, we treated hepatocytes with EGF and checked activation of downstream

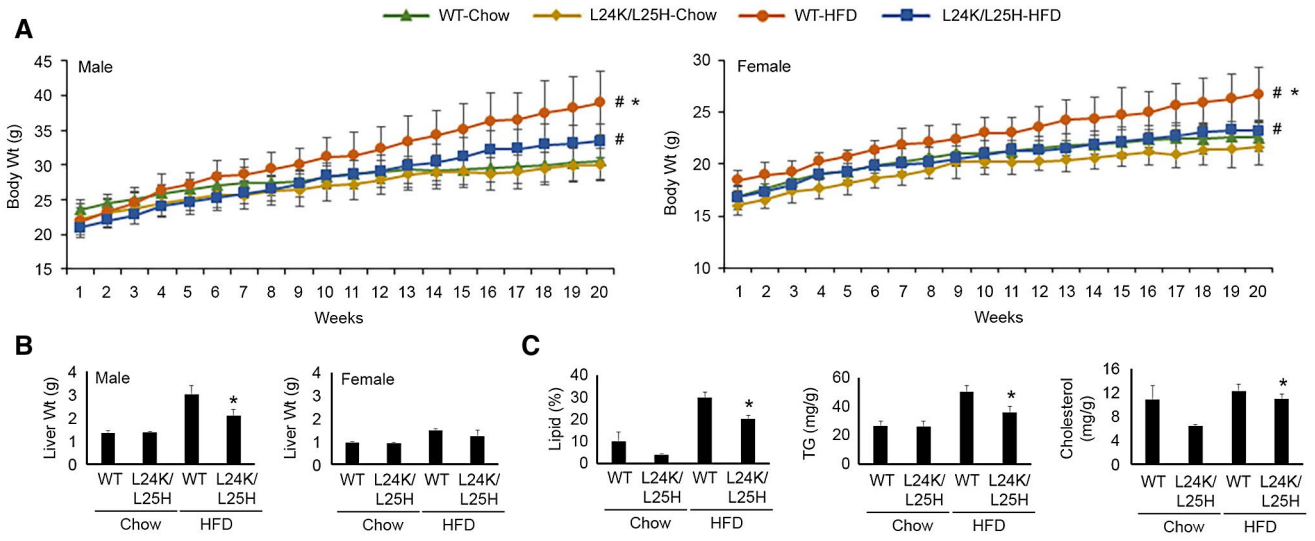

FIG. 5. AEG-1-L24K/L25H mice are partially protected from hepatic lipid accumulation upon HFD feeding. (A) Weekly body-weight measurement of chow-fed and HFD-fed male and female AEG-1-WT and AEG-1-L24K/L25H mice (n = 8 for each group). Data represent mean ± SEM. $^{\#}P < 0.05$ versus corresponding chow-fed mice; $^{*}P < 0.05$ versus HFD-fed AEG-1-L24K/L25H mice. (B) Measurement of liver weight at the end of the experiment (n = 8 for each group). Data represent mean ± SEM. $^{*}P < 0.05$ versus HFD-fed AEG-1-WT. (C) Measurement of hepatic lipid (left panel), TG (middle panel), and cholesterol (right panel) in male mice at the end of the experiment (n = 8 for each group). Data represent mean ± SEM. $^{*}P < 0.05$ versus HFD-fed AEG-1-WT.

mitogenic signaling molecules ERK and AKT. EGF-induced activation of ERK and AKT is significantly increased in AEG-1-L24K/L25H compared with AEG-1-WT (Fig. 4A,B). As a corollary, cell viability and BrdU incorporation were significantly higher and senescence was significantly lower in AEG-1-L24K/L25H hepatocytes compared with AEG-1-WT (Fig. 4C-E). It should be noted that primary mouse hepatocytes do not divide *in vitro* and start becoming senescent after 4 days of culture.

We next checked the response of AEG-1-WT and AEG-1-L24K/L25H littermates to HFD feeding. On chow diet, both male and female AEG-1-WT and AEG-1-L24K/L25H littermates did not show any difference in body and liver weights (Fig. 5A,B). On HFD in females, AEG-1-WT mice gained more body weight compared with AEG-1-L24K/L25H littermates but there was no significant difference in their liver weight, which might be due to inherent resistance of female C57BL/6 mice to HFD-induced steatosis (Fig. 5A,B). On HFD, male AEG-1-WT mice showed significant increase in body and liver weights when compared with chow-fed mice (Fig. 5A,B). This HFD-induced increase in body and liver weights was significantly blunted in male AEG-1-L24K/L25H mice compared with AEG-1-WT littermates (Fig. 5A,B). As a corollary, hepatic lipid content as well as cholesterol and TG levels were significantly less in HFD-fed male AEG-1-L24K/L25H mice compared with HFD-fed male AEG-1-WT littermates (Fig. 5C). Histological analysis revealed no anatomical abnormality in male and female chow-fed AEG-1-L24K/L25H livers compared with AEG-1-WT livers (Fig. 6; first and third rows). Steatosis assessment was performed following the Clinical Research Network NASH Scoring System.[23] Severe microvesicular and macrovesicular steatosis (grade 3, score: >66%) was observed in HFD-fed male AEG-1-WT livers, whereas AEG-1-L24K/L25H livers showed mild microvesicular and macrovesicular steatosis (grade 1, score 5%-33%) (Fig. 6, second row). Female mice showed very minimal microvascular steatosis in either group (Fig. 6, fourth row). Interestingly, both male and female AEG-1-L24K/L25H livers presented with leukocyte infiltrate versus their AEG-1-WT littermates, which was more pronounced in females, further demonstrating increased inflammation (arrows in Fig. 6). IHC analysis of HFD-fed male liver sections revealed intense staining for

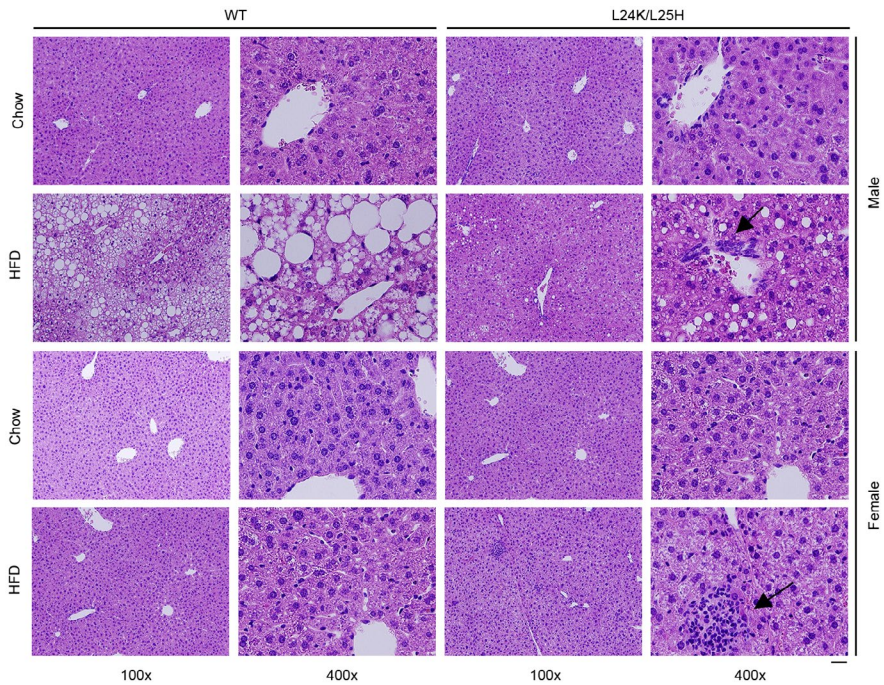

FIG. 6. AEG-1-L24K/L25H mice are partially protected from HFD-induced steatosis. AEG-1-WT and AEG-1-L24K/L25H mice were fed chow or HFD for 20 weeks. Hematoxylin and eosin staining of the liver sections at the end of the experiment. Scale bar: 20 μm. Arrows indicate leukocyte infiltration.

PLIN2, a marker of steatosis, in AEG-1-WT versus AEG-1-L24K/L25H (Fig. 7A,B). No difference in PLIN2 staining was observed in chow-fed livers (Supporting Fig. S1). Increased infiltration of macrophages and neutrophils was observed both in chow-fed and HFD-fed AEG-1-L24K/L25H compared with AEG-1-WT livers (Fig. 7A,B and Supporting Fig. S1).

Even though we observed increased activation of PPARα indicating increased FAO, we did not observe complete protection of AEG-1-L24K/L25H livers from HFD-induced steatosis. AEG-1 translationally regulates fatty acid synthesizing enzymes contributing to *de novo* lipogenesis (DNL).[6,17] Indeed, the levels of FA synthesizing enzymes, such as ACACA, FASN and stearoyl-coenzyme A desaturase 1/2 (SCD1/2), and cholesterol synthesizing enzymes, such as HMGCR and HMGCS1, were significantly higher in AEG-1-L24K/L25H hepatocytes versus AEG-1-WT (Fig. 7C,D). Additionally, the levels of SREBP1/2, transcription factors regulating FA and cholesterol synthesis, are significantly increased in AEG-1-L24K/L25H hepatocytes compared with AEG-1-WT (Fig. 7C,D). Cell cycle regulatory proteins CCND1 and cyclin E were also markedly increased in AEG-1-L24K/L25H hepatocytes versus AEG-1-WT, further indicating increased mitotic ability of the former (Fig. 7C,D). We hypothesized that AEG-1-L24K/L25H might exert increased binding to the mRNAs for lipogenic enzymes, resulting in increased translation. Indeed, RNA-IP followed by quantitative real-time PCR revealed increased binding of AEG-1-L24K/L25H to FASN mRNA compared with WT (Fig. 7E).

Discussion

Obesity is a global pandemic.[24] High fat and sugar containing diet is a key factor for obesity, which is closely associated with nonalcoholic fatty liver disease (NAFLD), the most common cause of chronic liver disease in the Western world, leading to cirrhosis and HCC.[25,26] NAFLD is characterized by initial accumulation of TG in hepatocytes (hepatic steatosis) with subsequent more advanced NASH marked by inflammation, hepatocyte injury and ballooning, and

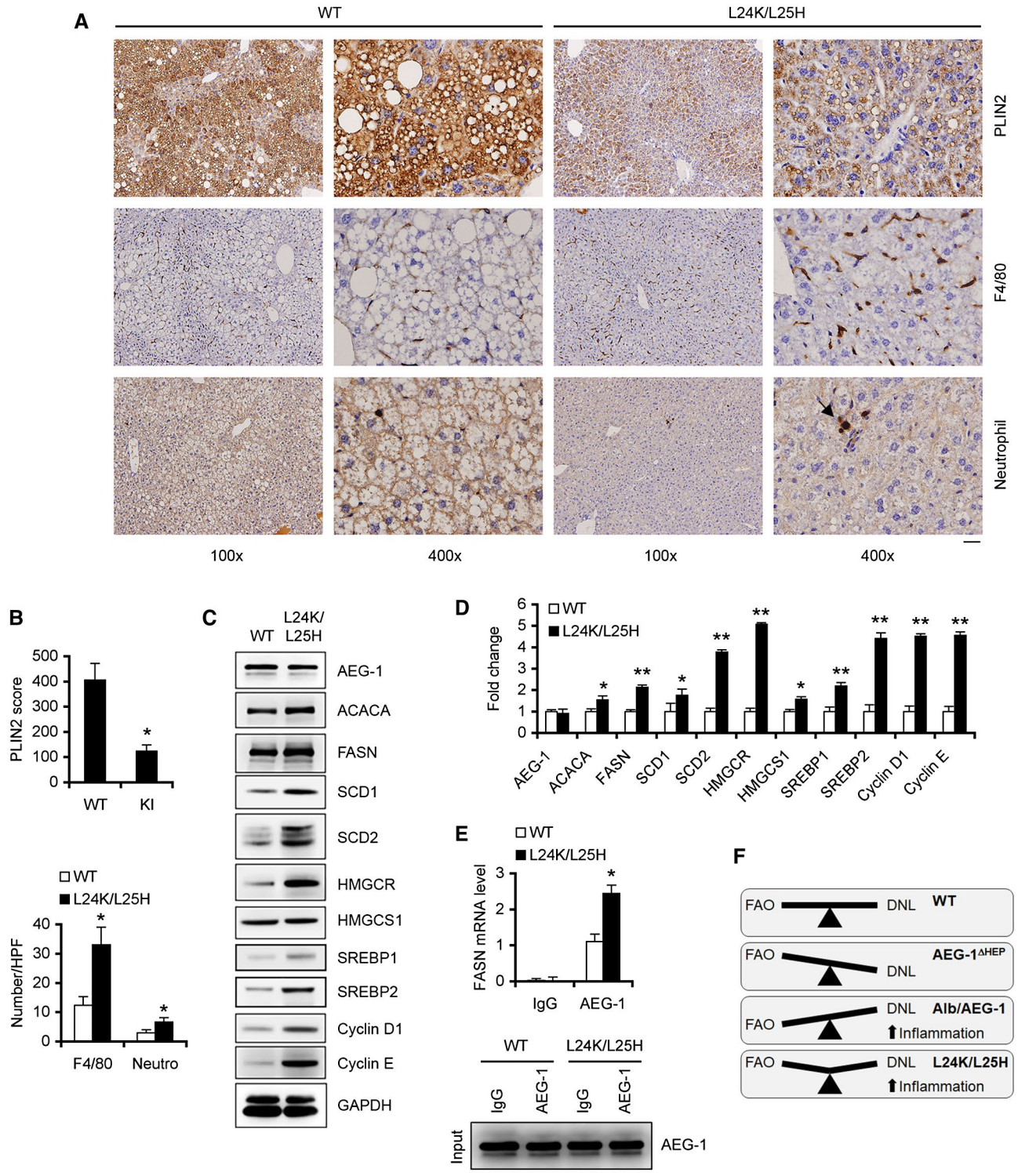

varying levels of fibrosis.[26] In obesity, free fatty acids are mobilized from adipose tissue and deposited in the liver.[26] Additionally, liver makes FAs by DNL using carbohydrates, primarily fructose, as substrate. Use of FAs by FAO is inhibited, therefore allowing the excess FAs to store as TGs in lipid droplets. Mechanistically, we documented that there are two ways that AEG-1 promotes steatosis. AEG-1 blocks PPARα activation,

FIG. 7. Inflammatory infiltrates and lipid synthesizing enzymes are increased in AEG-1-L24K/L25H livers. (A) Immunostaining for the indicated proteins in liver sections of male HFD-fed mice. F4/80 antibody stains macrophages. Scale bar: 20 μm. Arrow indicates neutrophil infiltration. (B) Top: Quantification of PLIN2 IHC score. Bottom, number of F4/80-positive macrophages and neutrophils per high power field. Data represent mean ± SEM. $^{*}P < 0.05$. (C) Representative western blot for the indicated proteins in AEG-1-WT and AEG-1-L24K/L25H hepatocytes. GAPDH was used as loading control. (D) Graphical representation of densitometric analysis of western blot shown in (C). Data represent mean ± SEM of at least triplicate independent experiments performed with hepatocytes isolated from littermates. $^{*}P < 0.05$; $^{**}P < 0.01$. (E) Top: Liver extracts from AEG-1-WT and AEG-1-L24K/L25H mice were subjected to IP using anti-AEG-1 antibody, and the levels of FASN mRNA in the immunoprecipitates were measured. Data represent mean ± SEM of triplicate independent experiments. $^{*}P < 0.01$. Bottom: Representative western blot for AEG-1 in 5% of the input documenting equal amounts of AEG-1 in each sample. (F) Cartoon showing events in mice with different AEG-1 status. In WT mice there is a balance between FAO and DNL. In AEG-1$^{\Delta HEP}$ mice, FAO is increased and DNL is decreased, which protects them from HFD-induced NASH. Alb/AEG-1 mice show decreased FAO and increased DNL as well as increased inflammation, resulting in spontaneous NASH. In AEG-1-L24K/L25H livers, both FAO and DNL are increased, which provides partial protection from HFD-induced steatosis, and there is also increased inflammation.

hence FAO.[17] As an ER membrane–anchored RNA-binding protein AEG-1 preferentially binds to mRNAs that code for fatty acid–synthesizing enzymes (e.g., FASN) and increases their translation, thus promoting DNL.[6,17] By activating NF-κB, AEG-1 promotes the inflammatory and fibrotic components of NASH.[17] Thus, AEG-1 augments every aspect of NASH by multiple mechanisms. We previously documented that in AEG-1$^{\Delta HEP}$ livers, FAO is increased and DNL is decreased, thus protecting from HFD-induced NASH and *vice versa* in Alb/AEG-1 livers along with increased inflammation, and thus inducing spontaneous NASH (Fig. 7F).[17] In AEG-1-L24K/L25H, both FAO and DNL are increased with augmentation of inflammation, thus creating a novel phenotype (Fig. 7F).

AEG-1 is a unique protein having diverse functional attributes mediated by diverse protein–protein and protein–RNA interactions. AEG-1-L24K/L25H mutant abolishes the ability of AEG-1 to inhibit nuclear receptor function, especially the ability to inhibit PPARα. In AEG-1-L24K/L25H hepatocytes, the basal and inducible expression of PPARα target genes, including the rate-limiting transporter of FAO Cpt1a, is significantly higher compared with AEG-1-WT hepatocytes. As a consequence, FAO should be higher in AEG-1-L24K/L25H hepatocytes, thus protecting from HFD-induced steatosis. Indeed, the degree of steatosis and hepatic TG accumulation is significantly lower in AEG-1-L24K/L25H livers compared with AEG-1-WT livers. However, AEG-1-L24K/L25H livers are not completely protected from HFD-induced steatosis. We observe that the levels of FA-synthesizing enzymes are significantly higher in AEG-1-L24K/L25H livers versus AEG-1-WT livers contributing to DNL, which might explain why despite the increased FAO, AEG-1-L24K/L25H livers are not completely protected from HFD-induced steatosis.

As an oncogene, AEG-1 is overexpressed in all cancers as yet studied, and approximately 90% of patients with HCC show AEG-1 overexpression by a variety of mechanisms including genomic amplification.[4,27] In HCC cells there are many copies of AEG-1 gene compared with primary hepatocytes. It is interesting that even at equal gene-dosage level, AEG-1-L24K/L25H could significantly activate tumorigenic molecules and augment tumorigenic pathways compared with AEG-1-WT. Similarly, AEG-1 is a known activator of NF-κB and inflammation, and AEG-1-L24K/L25H acquired a dominant positive function over AEG-1-WT in activating these pathways. These observations suggest that when AEG-1-L24K/L25H loses its ability to interact with nuclear receptors, it becomes free to interact with other molecules, resulting in "gain-of-function" attributes compared with AEG-1-WT. Indeed, AEG-1-L24K/L25H mutant showed increased binding to p65 NF-κB or FASN mRNA, and increased activation of ERK and AKT compared with AEG-1-WT. Therefore, even though LXXLL motif facilitates NASH development by AEG-1, the same motif also restricts further oncogenic functions of AEG-1, so that the predisposing condition NASH does not rapidly develop into HCC. This balance is overwhelmed when high levels of AEG-1 start accumulating in a transformed cell, resulting in frank HCC development.

In summary, our observations unravel the unique role of the small LXXLL motif in mediating the balance between the metabolic and oncogenic functions

of AEG-1. AEG-1 is being increasingly appreciated as a viable target for ameliorating NASH and NASH-HCC, and as such, in-depth understanding of the functions and molecular attributes of this molecule is essential. The present studies take us one step further in this understanding.

REFERENCES

1) Evans RM, Mangelsdorf DJ. Nuclear receptors, RXR, and the Big Bang. Cell 2014;157:255-266.
2) Heery DM, Kalkhoven E, Hoare S, Parker MG. A signature motif in transcriptional co-activators mediates binding to nuclear receptors. Nature 1997;387:733-736.
3) Sarkar D, Fisher PB. AEG-1/MTDH/LYRIC: clinical significance. Adv Cancer Res 2013;120:39-74.
4) Yoo BK, Emdad L, Su Z-Z, Villanueva A, Chiang DY, Mukhopadhyay ND, et al. Astrocyte elevated gene-1 regulates hepatocellular carcinoma development and progression. J Clin Invest 2009;119:465-477.
5) Srivastava J, Robertson CL, Rajasekaran D, Gredler R, Siddiq A, Emdad L, et al. AEG-1 regulates retinoid X receptor and inhibits retinoid signaling. Cancer Res 2014;74:4364-4377.
6) Hsu JC, Reid DW, Hoffman AM, Sarkar D, Nicchitta CV. Oncoprotein AEG-1 is an endoplasmic reticulum RNA binding protein whose interactome is enriched in organelle resident protein-encoding mRNAs. RNA 2018;5:688-703.
7) Brown DM, Ruoslahti E. Metadherin, a cell surface protein in breast tumors that mediates lung metastasis. Cancer Cell 2004;5:365-374.
8) Thirkettle HJ, Girling J, Warren AY, Mills IG, Sahadevan K, Leung H, et al. LYRIC/AEG-1 is targeted to different subcellular compartments by ubiquitinylation and intrinsic nuclear localization signals. Clin Cancer Res 2009;15:3003-3013.
9) Sarkar D, Park ES, Emdad L, Lee SG, Su ZZ, Fisher PB. Molecular basis of nuclear factor-kappaB activation by astrocyte elevated gene-1. Cancer Res 2008;68:1478-1484.
10) Alexia C, Poalas K, Carvalho G, Zemirli N, Dwyer J, Dubois SM, Hatchi EM, et al. The endoplasmic reticulum acts as a platform for ubiquitylated components of nuclear factor kappaB signaling. Sci Signal 2013;6:ra79.
11) Krishnan RK, Nolte H, Sun T, Kaur H, Sreenivasan K, Looso M, et al. Quantitative analysis of the TNF-alpha-induced phosphoproteome reveals AEG-1/MTDH/LYRIC as an IKKbeta substrate. Nat Commun 2015;6:6658.
12) Robertson CL, Srivastava J, Siddiq A, Gredler R, Emdad L, Rajasekaran D, et al. Genetic deletion of AEG-1 prevents hepatocarcinogenesis. Cancer Res 2014;74:6184-6193.
13) Meng X, Zhu D, Yang S, Wang X, Xiong Z, Zhang Y, et al. Cytoplasmic Metadherin (MTDH) provides survival advantage under conditions of stress by acting as RNA-binding protein. J Biol Chem 2012;287:4485-4491.
14) Lefebvre P, Benomar Y, Staels B. Retinoid X receptors: common heterodimerization partners with distinct functions. Trends Endocrinol Metab 2010;21:676-683.
15) Srivastava J, Robertson CL, Gredler R, Siddiq A, Rajasekaran D, Akiel MA, et al. Astrocyte elevated gene-1 (AEG-1) contributes to non-thyroidal illness syndrome (NTIS) associated with hepatocellular carcinoma (HCC). J Biol Chem 2015;290:15549-15558.
16) Robertson CL, Srivastava J, Siddiq A, Gredler R, Emdad L, Rajasekaran D, et al. Astrocyte elevated gene-1 (AEG-1) regulates lipid homeostasis. J Biol Chem 2015;290:18227-18236.
17) **Srivastava J**, **Robertson CL**, Ebeid K, Dozmorov M, Rajasekaran D, Mendoza R, et al. A novel role of astrocyte elevated gene-1 (AEG-1) in regulating nonalcoholic steatohepatitis (NASH). Hepatology 2017;66:466-480.
18) Kersten S. Integrated physiology and systems biology of PPARalpha. Mol Metab 2014;3:354-371.
19) Hsu PD, Lander ES, Zhang F. Development and applications of CRISPR-Cas9 for genome engineering. Cell 2014;157:1262-1278.
20) Srivastava J, Siddiq A, Emdad L, Santhekadur PK, Chen D, Gredler R, et al. Astrocyte elevated gene-1 promotes hepatocarcinogenesis: novel insights from a mouse model. Hepatology 2012;56:1782-1791.
21) Akiel M, Guo C, Li X, Rajasekaran D, Mendoza RG, Robertson CL, et al. IGFBP7 deletion promotes hepatocellular carcinoma. Cancer Res 2017;77:4014-4025.
22) Robertson CL, Mendoza RG, Jariwala N, Dozmorov M, Mukhopadhyay ND, Subler MA, et al. Astrocyte elevated gene-1 regulates macrophage activation in hepatocellular carcinogenesis. Cancer Res 2018;78:6436-6446.
23) Kleiner DE, Brunt EM, Van Natta M, Behling C, Contos MJ, Cummings OW, et al. Design and validation of a histological scoring system for nonalcoholic fatty liver disease. Hepatology 2005;41:1313-1321.
24) Jaacks LM, Vandevijvere S, Pan AN, McGowan CJ, Wallace C, Imamura F, et al. The obesity transition: stages of the global epidemic. Lancet Diabetes Endocrinol 2019;7:231-240.
25) Anstee QM, Reeves HL, Kotsiliti E, Govaere O, Heikenwalder M. From NASH to HCC: current concepts and future challenges. Nat Rev Gastroenterol Hepatol 2019;16:411-428.
26) Friedman SL, Neuschwander-Tetri BA, Rinella M, Sanyal AJ. Mechanisms of NAFLD development and therapeutic strategies. Nat Med 2018;24:908-922.
27) Sarkar D. AEG-1/MTDH/LYRIC in liver cancer. Adv Cancer Res 2013;120:193-221.

Author names in bold designate shared co-first authorship.

Supporting Information

Additional Supporting Information may be found at onlinelibrary.wiley.com/doi/10.1002/hep4.1834/suppinfo.